Available online at www.sciencedirect.com
SCIENCE DIRECT
Journal of Solid State Chemistry 179 (2006) 2120–2125
JOURNAL OF SOLID STATE CHEMISTRY
www.elsevier.com/locate/jssc

# Electronic, magnetic and structural properties of $A_2VMoO_6$ perovskites ($A$ = Ca, Sr)

P. Karen[a,*], A.R. Moodenbaugh[b], J. Goldberger[c,1], P.N. Santhosh[c,2], P.M. Woodward[c]

[a]Department of Chemistry, University of Oslo, P.O. Box 1033 Blindern N-0315, Oslo, Norway
[b]Condensed Matter Physics & Materials Science Department, Brookhaven National Laboratory, Upton, NY 11973-5000, USA
[c]Department of Chemistry, Ohio State University, 100 West 18th Avenue, Columbus, OH 43210-1185, USA

Received 23 February 2006; received in revised form 4 April 2006; accepted 5 April 2006
Available online 25 April 2006

**Abstract**

The perovskites $Sr_2VMoO_6$ and $Ca_2VMoO_6$ have been synthesized by liquid-mix technique in citrate melts, and their electronic, magnetic and structural properties have been investigated. No signs of V/Mo ordering are seen by synchrotron X-ray powder diffraction, but despite the chemical disorder both oxides are highly conductive and Pauli paramagnetic. Electrical conductivities of these solid solutions are comparable or higher than those reported for polycrystalline $AMoO_3$ end members. It is suggested that the delocalized metallic conductivity of these compounds with two different transition-metal atoms implies valence equilibrium between the degenerate oxidation-state couples $V^{4+}Mo^{4+}$ and $V^{3+}Mo^{5+}$.


*Keywords:* Metallic perovskite oxides; Pauli paramagnetic oxides

## 1. Introduction

Among conducting oxides those compounds which adopt the perovskite structure are disproportionately represented. This is due in part to the fact that the high symmetry of the perovskite structure produces a highly disperse conduction band. Thus for appropriate electron counts mobile carriers and delocalized electronic transport are expected. Furthermore, perovskite structures readily accommodate oxygen defects so that ionic conductivity can and does develop. Those perovskites that exhibit both electronic and ionic conductivity are attractive for applications as anodes or cathodes in solid-oxide fuel cells, as well as for semi-permeable membranes for oxygen separation from gas mixtures.

Although there are many perovskites that are well conducting, relatively few of these oxides are truly metallic. The necessary (yet not sufficient) condition for metallic behavior in a transition-metal perovskite is an intermediate valence state of high covalency [1], as an example, tetravalent ruthenium in ferromagnetic $SrRuO_3$. Other perovskites that exhibit metallic conductivity are for example $SrVO_3$ and $SrMoO_3$; both of which are Pauli paramagnetic [2,3]. The same is valid for their calcium variants [2,4]. With room-temperature conductivity of $\sim 2 \times 10^5$ S/cm, single-crystalline $SrMoO_3$ is reported [5] to have the highest electrical conductivity of any known oxide. In fact, this conductivity is two times that of Pt or Fe. An increasingly important area of application for metallic perovskites is their use as substrates for epitaxial growth in multilayer electronic devices that contain other types of functional perovskites.

In this study, we synthesized 1:1 solid solutions of these alkaline-earth vanadium and molybdenum perovskite oxides in order to see whether a sufficient V/Mo orbital mixing allows both solid solutions to remain metallic and Pauli paramagnetic. The advantage of combining two redox-prone transition-metal states in an oxide is that it widens the stability range in terms of equilibrium partial pressures of oxygen [6]. This feature could make

*Corresponding author. Fax: +47 228 554 41.
*E-mail address:* pavel.karen@kjemi.uio.no (P. Karen).
[1]Present address: Department of Chemistry, University of California, Berkeley, CA 94720, USA.
[2]Present address: Department of Physics, Indian Institute of Technology, Madras, Chennai 600 036, India.

0022-4596/$ - see front matter © 2006 Elsevier Inc. All rights reserved.
doi:10.1016/j.jssc.2006.04.013

these materials attractive for electrode applications in certain environments. In addition, formation of the solid solution would allow tuning unit-cell parameters by varying the V/Mo as well as Ca/Sr proportions. This may have a practical application for allowing greater flexibility in lattice matching of substrates for epitaxial growth.

While there is no prior report of $Ca_2VMoO_6$, the Sr variant has been synthesized and reported as a cubic perovskite with metallic conductivity above ambient temperatures [7]. However, the magnetic properties and low-temperature conductivity have not been previously examined and are reported here. In order to carefully look for the presence of long-range ordering of V and Mo in the title phases, we have utilized synchrotron X-ray powder diffraction to investigate the structural characteristics of these materials.

## 2. Experimental

### 2.1. Synthesis

$Sr_2VMoO_6$ and $Ca_2VMoO_6$ were synthesized from amorphous precursors obtained via liquid-mixing procedure in melted citric acid monohydrate. In order to produce roughly 30 g of $Sr_2VMoO_6$, 350 g of high-purity citric acid monohydrate (Fluka, reagent grade, $<0.02\%$ sulfate ash) was melted together with $\sim$50 mL of redistilled water in a 2 L beaker. Strontium was added to as a nitrate (Fluka, reagent grade) in concentrated solution. Then $NH_4VO_3$ (Merck, reagent grade, $V_2O_5$ assay by gravimetry) and $(NH_4)_6Mo_7O_{24}\cdot 4H_2O$ (Baker Analyzed) were dissolved together into a saturated solution. About 5 mL of this solution was carefully added into the boiling citrate/citric-acid solution on a magnetic hot-plate stirrer, with the effect of starting the reduction of the nitrate ions by the citric acid. After the vigorous evolution of nitrous gasses ceased, the rest of the vanadate and molybdate solution was added. The procedure for $Ca_2VMoO_6$ was analogous, except that calcium was added as $CaCO_3$ (reagent grade) in the last step, after the evolution of nitrous gasses has ceased, and dissolved upon addition of a small amount of (redistilled) water. In both cases, the resulting dark blue transparent liquid was evaporated to dryness in a drying oven at 170 °C. The formed porous xerogel was crushed to powder and slowly incinerated in a tall porcelain crucible with lid at 390 °C. The Ca-containing precursor was calcined overnight at 770 °C in $H_2$ gas (99.997% purity, 4 ppm $H_2O$, 3 ppm $O_2$). The Sr-containing precursor was calcined at 870 °C in a commercial gas mixture of 10.5% $H_2$ in Ar (99.999%, with certified analysis), humidified in a saturated solution of KBr at ambient temperature. The calcinations produced perovskite-type phases (with broad Bragg lines) of dark violet color. After homogenizations in a vibration mill, pellets were pressed (160 bar), and fired for 20–30 h at various temperatures in flowing argon-based atmospheres of controlled low partial pressure of oxygen (Table 1). The resulting porosities were assessed by weighing a sample of a regular geometrical shape.

Table 1
Reaction conditions of the $A_2MoVO_{6+w}$ sintering to the specified porosity and the resulting $w$ according to cerimetric titration

| $A$ | Sintering in argon-based atmospheres | | | | The product | |
|---|---|---|---|---|---|---|
| | $t$ (°C) | $H_2$ (%) | $H_2O$ (%) | $\log p_{O2}$ (bar) | Porosity (%) | $w$ |
| Ca | 1200 | 10.3 | 1.97 | −13.1 | 48 | 0.003(2) |
| | 1300 | 9.33 | 1.96 | −11.9 | 16 | 0.037(1) |
| Sr | 1200 | 10.3 | 1.99 | −13.1 | 67 | 0.025(1) |
| | 1350 | 10.3 | 2.09 | −11.5 | 44 | 0.017(3) |

### 2.2. Nonstoichiometry analysis

The average oxygen nonstoichiometry of the sample (assuming ideal stoichiometry for the metals) was determined by cerimetric titration of $Fe^{2+}$ formed upon oxidation of the sample into hexavalent molybdenum by an acidic solution of $FeCl_3$. Approximately 0.2 g of powdered sample in an Ar-flushed glass ampoule was added to 1 mL 1 M $FeCl_3$, 3 mL water and 5 mL of concentrated HCl in the said order. The ampoule was sealed and warmed to $\sim$50 °C. In less than 1 min, a clear solution was obtained. After cooling down, it was titrated cerimetrically with ferroin as an indicator.

### 2.3. X-ray diffraction

Powder X-ray diffraction data for characterization of all synthesis steps were obtained with a focussing Guinier–Hägg camera with Cu $K\alpha_1$ radiation and Si as an internal standard. For the least nonstoichiometric samples, synchrotron X-ray powder diffraction (SXPD) was performed at the X7A beamline located at the National Synchrotron Light Source at Brookhaven National Laboratory. Data were collected at 300 K, with a linear position-sensitive detector, over an angular range of 5–50° $2\theta$, on samples sealed in glass capillaries of 0.3 mm in diameter, in radiation of $\lambda = 0.695156$ Å (with 0.006% of a $\lambda/2$ contribution) obtained from a focusing Si 220 monochromator. The powder sample density was estimated to correct the data for absorption. Refinements of the crystal and magnetic structures were performed using the Rietveld method as implemented in the GSAS software suite [8]. A linear interpolation of fixed points was used to model the background. CIF files can be obtained from the Fachinformationszentrum Karlsruhe, 76344 Eggenstein-Leopoldshafen, Germany, (fax: (49)7247 808 666; e-mail: crysdata@fiz-karlsruhe.de) on quoting the depository number CSD 416201 for $Ca(V_{0.5}Mo_{0.5})O_3$ and CSD 416202 for $Sr(V_{0.5}Mo_{0.5})O_3$.

### 2.4. Electrical conductivity and magnetic susceptibility measurements

Electrical conductivity measurements were performed in the temperature range 10–300 K of the He-cryostat, using a linear four-probe method. Leads were attached to the regularly shaped bars using silver paint. Magnetization measurements were carried out using a Quantum Design MPMS magnetometer in a temperature range of 5–350 K on irregularly shaped sintered pellets of 20–60 mg mass. Zero-field cooled (ZFC) measurements were performed after samples had been brought from room temperature to ~5 K in a very low magnetic field $H \approx 0.5$ G, and a measuring field of typically $H = 100$ G was then applied. ZFC magnetization data were monitored upon warming, with each data point being measured after the temperature had stabilized. Field cooled (FC) measurements were performed on cooling in the applied field, temperature being controlled in the "undercool off" mode to minimize the effect of temperature hysteresis.

## 3. Results

### 3.1. Formation and characterization

The preparations were single phase according to synchrotron X-ray diffraction. Assuming the metal stoichiometry entered in the synthesis from standardized or analyzed chemicals, the average nominal oxygen contents of the sintered products are listed in Table 1, together with details on temperature and composition of the flowing reaction atmospheres.

The reaction conditions listed in Table 1 are close to the limit for oxidative decomposition of the title phases. Accordingly, the analyzed oxygen contents correspond to an oxygen excess, which, however, in perovskite-type structures is likely to be achieved by formation of metal vacancies. The nominal formulae in Table 1 need to be interpreted as confirmations that the synthesized phases are approaching stoichiometry from the side of oxidation, and that practically no reduced valence states are to be expected. For further illustration of the synthesis conditions consider the following. When the limit for the oxidative decomposition is crossed, for example by decreasing the hydrogen content in argon from ~10% by volume [$\log(p_{O_2}/\text{bar}) = -12.3$] used for the synthesis of $Ca_2VMoO_6$ to 1.4% [$\log(p_{O_2}/\text{bar}) = -10.7$], a completely fused mixture of $CaMoO_4$ and $CaVO_3$ is obtained at 1250 °C.

### 3.2. Crystal structure

For both phases, the samples with lowest oxygen nonstoichiometry (Table 1) were used for SXPD. The nonstoichiometry has been neglected in the subsequent Rietveld refinements, owing to its low level and the ambiguity of distinguishing between low concentrations of metal vacancies versus oxygen interstitials as alternatives. No signs of ordering of V and Mo atoms into a supercell are seen in SXPD patterns of either phase. The crystal structure of $Sr_2VMoO_6$ is that of the undistorted cubic perovskite (space group $Pm-3m$, $a = 3.91581 \pm 3$ Å), in agreement with data in Ref. [7] obtained by conventional X-ray powder diffraction. In order to accommodate the divalent calcium ion, which is smaller than strontium, the structure of $Ca_2VMoO_6$ undergoes an octahedral tilting distortion, which lowers the symmetry to the orthorhombic *Pnma* space group. Among the various types of octahedral tilting distortions this type (designated as $a^-b^+a^-$ in Glazer notation [9]) is the most common, occurring at ambient conditions in more than half of all perovskites [10] (Fig. 1). The refined structural parameters for $Ca_2VMoO_6$ are given in Table 2.

### 3.3. Electrical conductivity

Fig. 2 shows that electrical conductivities of both $Ca_2VMoO_6$ and $Sr_2VMoO_6$ are very high and increase with decreasing temperature. This behavior is typical of compounds exhibiting metallic conductivity. The high porosity (44%) of the $Sr_2VMoO_6$ sample, as well as difficulties of resistance measurements on such a highly conducting material, contributed to the scatter of data in Fig. 2. However, the conductivity decrease observed below

Table 2
The refined structure of $Ca_2VMoO_6$ at 298 K, as obtained from SXPD data ($\lambda = 0.695156$ Å)

| Atom | Site | $x$ | $y$ | $z$ | $U_{iso} \times 100$ (Å$^2$) |
|---|---|---|---|---|---|
| Ca | 4*c* | 0.0354(2) | 1/4 | –0.0063(4) | 1.11(2) |
| V/Mo | 4*b* | 0.5 | 0 | 0 | 0.33(1) |
| O(1) | 4*c* | 0.4841(8) | 1/4 | 0.0750(7) | 1.14(12) |
| O(2) | 8*d* | 0.2876(5) | 0.0357(4) | 0.7124(5) | 0.39(7) |

The space group symmetry is *Pnma*, and the unit cell dimensions are $a = 5.46613(8)$ Å, $b = 7.6822(1)$ Å and $c = 5.40335(7)$ Å. The figures of merit are $R_{wp} = 0.0406$, fitted $R_p = 0.0290$, $R(F^2) = 0.0277$, based on 258 reflections and 20 variables.

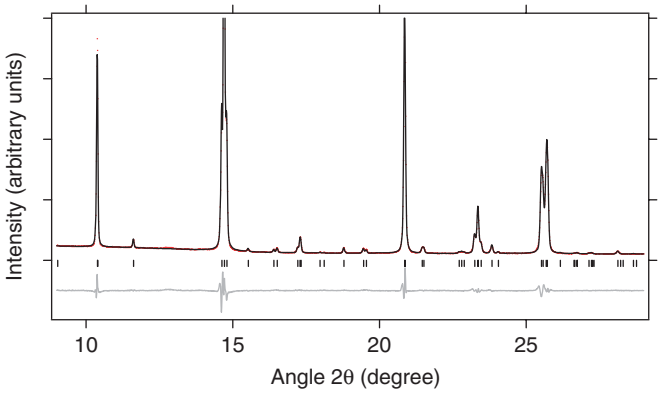


Fig. 1. Rietveld fit for $Ca_2VMoO_6$ (50% along both scales is shown).

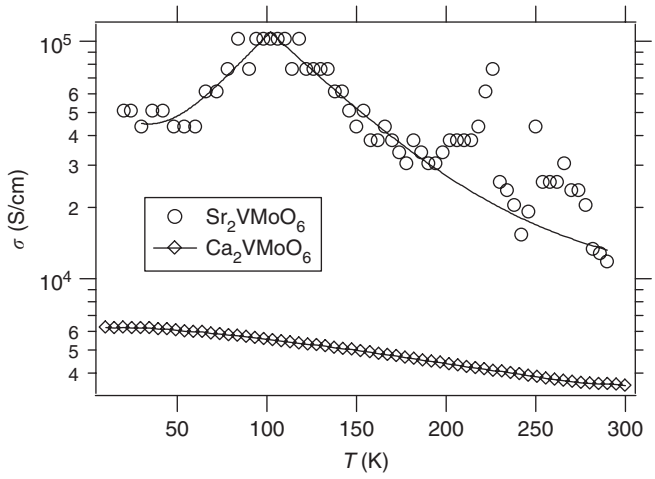


Fig. 2. Electrical conductivities ($\sigma$) vs. temperature for polycrystalline $Ca_2VMoO_{6.037(1)}$ and $Sr_2VMoO_{6.017(3)}$ samples.

some 100 K appears real and should be attributed to contribution from activated grain-boundary resistance, which prevails upon cooling. It is seen that formation of such a temperature-independent range upon cooling starts at lower temperatures for the Ca-based sample of only 16% porosity. This approaches behavior of polycrystalline malleable metals, where the grain-boundary contribution is even smaller. Attempts to measure the conductivity of the more porous (48%) yet on average less nonstoichiometric sample $Ca_2VMoO_{6.003(2)}$ resulted into rather scattered values that were equal or somewhat larger than those shown for $Ca_2VMoO_{6.037(2)}$ in Fig. 2. This suggests that variations in the oxygen excess $w$ do not have large effect on conductivity of $Ca_2VMoO_{6+w}$.

### 3.4. Magnetometry

Magnetic susceptibility ($\chi$) measurements as a function of temperature ($T$) were collected both in the ZFC and FC regime using an applied field of 100 G. Fig. 3 shows both types of data for $Ca_2VMoO_6$ and $Sr_2VMoO_6$.

$Ca_2VMoO_6$ shows a weak, temperature-independent susceptibility typical of Pauli paramagnetism. Such a behavior is consistent with metallic conductivity of this phase. The constant susceptibility of $7.024(1) \times 10^{-4}$ emu/Oe was obtained by extrapolation to 0 K of ZFC molar susceptibility data from above 100 K, as shown in Fig. 3 top. After correction for diamagnetism of core electrons, $\chi_{core} = -1.12 \times 10^{-4}$ emu/Oe per formula unit, calculated from atomic values listed in Ref. [11], an estimate is obtained for the total susceptibility (diamagnetic Landau and paramagnetic Pauli) of conduction electrons per mol $Ca_2VMoO_6$: $\chi_{lp} = 8.14 \times 10^{-4}$ emu/Oe. This value is somewhat larger than the sum of the reported net paramagnetic susceptibilities per mol of $CaVO_3$ ($2.8 \times 10^{-4}$ emu/Oe [12], or $4.4 \times 10^{-4}$ emu/Oe [2]) and $CaMoO_3$ ($2.5 \times 10^{-4}$ emu/Oe [4]). When the electron-mass enhancement $m_e^*/m_e$ associated with band-structure effects is neglected, the Landau

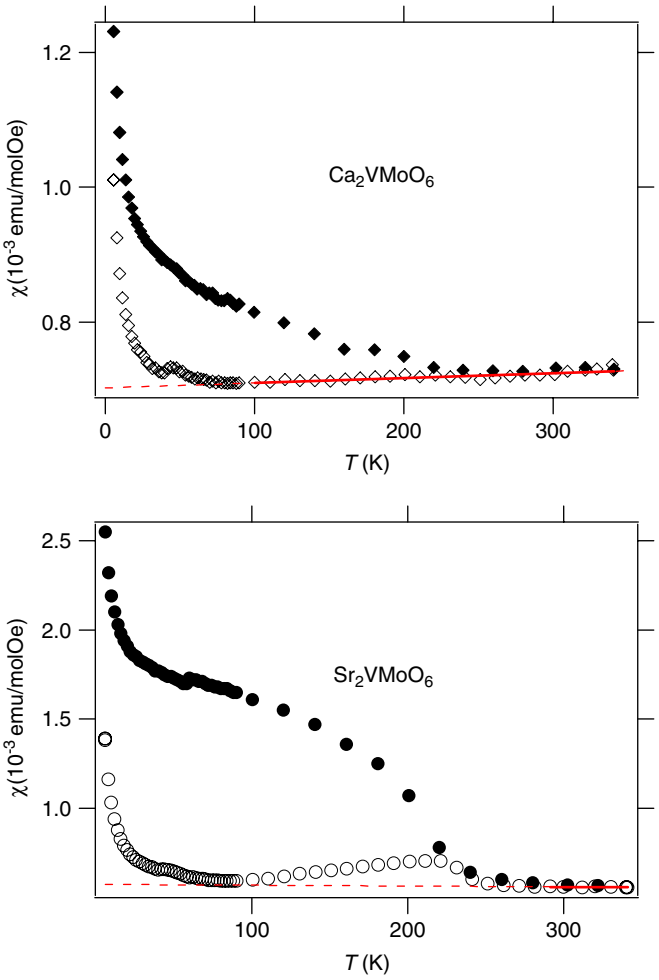


Fig. 3. Field-cooled (●) and zero-field cooled (○) magnetic susceptibility vs. temperature for the $Ca_2VMoO_{6.003(2)}$ and $Sr_2VMoO_{6.017(3)}$ samples.

diamagnetic susceptibility is one third of the magnitude of the Pauli paramagnetic susceptibility, and $\chi_{pp} = 1.2 \times 10^{-3}$ emu/Oe is hence obtained as an upper estimate for Pauli paramagnetic susceptibility per mol of $Ca_2VMoO_6$. When the electron-mass enhancement is considered, the ideal 1/3 ratio of the magnitudes of the Landau diamagnetic and Pauli paramagnetic contributions is scaled by a factor of $(m_e/m_e^*)^2$. Because $m_e^*/m_e > 1$ is evaluated from specific-heat measurements in similar phases such as $CaVO_3$ [13], the $\chi_{lp}$ value may be considered the minimum estimate.

There is a Curie-like increase in susceptibility for both ZFC (below 70 K) and FC (below 250 K) measurements. Analogous behavior is seen for similar Pauli-paramagnetic oxides, for example the end members of the title solid solutions: $CaVO_3$ [12] and $SrMoO_3$ [14] and is attributed to the presence of residual localized valence electrons. Also aliovalent point defects undoubtedly contribute to this paramagnetism, and traces of magnetic impurities cannot be excluded. Also the hysteresis observed between the ZFC and FC data sets suggests a ferromagnetic, ferrimagnetic or spin-glass like contribution.

Magnetic susceptibility of $Sr_2VMoO_6$ is also practically constant as a function of temperature (Fig. 3 bottom). There is even greater evidence of the presence of trace magnetic defects in this sample. This statement is based on the observation that the magnetization maximum at 220 K on the ZFC curve was poorly reproducible, varying by tens of Kelvin from measurement to measurement. The Pauli paramagnetic behavior of $Sr_2VMoO_6$ was analyzed in the same manner as described above for $Ca_2VMoO_6$, using the 290–350 K ZFC molar susceptibility data to determine the constant susceptibility of $5.56(1)\times10^{-4}$ emu/Oe per formula unit. The constant susceptibility corrected for diamagnetism of the core electrons is close to the sum of such molar values for $SrVO_3$ ($2.80\times10^{-4}$ emu/Oe [15]) and $SrMoO_3$ ($2.15\times10^{-4}$ emu/Oe [3]). Again, only a rough estimate was possible for the Pauli paramagnetic susceptibility, giving $\chi_{pp}\approx1.0\times10^{-3}$ emu/Oe when $m_e^*/m_e=1$; a value similar to that obtained for $Ca_2VMoO_6$.

## 4. Discussion

In Table 3, electrical conductivities at 290 K from Fig. 2 are compared with those reported for the end-member phases of the title solid solutions. It is seen that the electrical conductivity of the V, Mo solid solution is at least as high as that of the Mo-based end member whereas conductivities of the V-based perovskites are lower, despite being metallic and Pauli paramagnetic as well. When Ca replaces Sr, the octahedral tilting distortion decreases the M–O–M angles from the 180° value found in the cubic perovskite structure. This structural distortion decreases the orbital overlap between the metal *d*-orbitals and the oxygen 2*p* orbitals, which leads to a decrease in the conduction band width and a corresponding decrease in electrical conductivity [16]. Because the 3*d* orbitals of the vanadium ion are smaller than the 4*d* orbitals of the molybdenum ion, the effect of the octahedral tilting on the electrical conductivity is more pronounced in the $AVO_3$ series ($A$ = Sr, Ca), where the conductivity decreases by roughly five orders of magnitude upon replacing strontium with calcium, than it is in $AMoO_3$ series, where the conductivity only decreases by roughly one order of magnitude. Interestingly, in the V/Mo solid solution the drop in conductivity (~70%) associated with the octahedral tilting distortion is even smaller, even though the structural distortion is comparable.

Table 3
Comparison of room-temperature electrical conductivities, bond distances and bond angles for the title phases $A_2VMoO_6$ and their solid-solution end members

| $A$ | $AVO_3$ | $A_2VMoO_6$ | $AMoO_3$ |
|---|---|---|---|
| Ca | | | |
| $\sigma$ (S/cm) | $2.9\times10^{-2}$ | $3.6\times10^{3}$ | $8.5\times10^{2}$ |
| Porosity | Not reported | 16% | 38% |
| Reference | [12] | This study | [17] |
| $M$–O distances (Å) | 2 × 1.9121(5) [O(1)] | 2 × 1.965(1) [O(1)] | |
| | 2 × 1.920(2) [O(2)] | 2 × 1.959(3) [O(2)] | |
| | 2 × 1.913(2) [O(2)] | 2 × 1.966(3) [O(2)] | |
| $M$–O–$M$ angles (°) | 161.33(2) [O1] | 155.64(0) [O1] | |
| | 159.16(3) [O2] | 156.6(2) [O2] | |
| Reference | [12] | This study | |
| Sr | | | |
| $\sigma$ (S/cm) | $4.0\times10^{2}$ | $1.2\times10^{4}$ | $1.0\times10^{4}$ |
| Porosity | 15–20% | 44% | 54% |
| Reference | [18] | This study | [17] |
| $M$–O dist. (Å) | 1.9212(1) | 6 × 1.95791(1) | 1.9876 |
| $M$–O–$M$ angles (°) | 180 | 180 | 180 |
| Reference | [2] | This study | [19] |

The fact that the conductivities of the studied V/Mo solid solution phases are comparable with those of the corresponding ternary Mo oxides suggests that a pure single-crystalline $Sr_2VMoO_6$ is one of the highest conducting oxides recorded to date. Although the polycrystalline oxides are rather poorly sinterable at typical synthesis temperatures from carbonate precursors, for some applications the high surface and low sinterability would be an added benefit. The metallic conductivity and Pauli paramagnetism of $Sr_2VMoO_6$ and $Ca_2VMoO_6$ leave little doubt that the *d*-electrons of these two transition metals are highly delocalized. This behavior further suggests a considerable energetic overlap of the vanadium and molybdenum $t_{2g}$ orbitals. The delocalized metallic conductivity of these compounds with two different transition-metal atoms implies valence equilibrium between the degenerate oxidation-state couples $V^{4+}Mo^{4+}$ and $V^{3+}Mo^{5+}$. Such an assignment is also consistent with the observed V/Mo–O bond distances (Table 3): The expected average transition metal–oxygen distance, based upon Shannon radii [20] (assuming a coordination number of two for the oxygen, as is most accurate for perovskites), is 1.965 Å for $V^{4+}/Mo^{4+}$ and 1.975 Å for $V^{3+}/Mo^{5+}$. The very small difference between ionic radii for the alternative $t_{2g}$ configurations is at least partially responsible for the fact that electron transport in these compounds shows little sign of coupling with the lattice. Hence metallic conductivity rather than polaronic transport is observed. Given the full miscibility of $SrMoO_3$ and $SrVO_3$ [7] and cubic symmetry up to $x=0.25$ in $(Ca_xSr_{1-x})VO_3$ [21], an array of cubic metallic substrates can be tailored for perovskite epitaxy, with unit-cell parameters ranging from 3.83 Å [21] for $Ca_{0.25}Sr_{0.75}VO_3$ to 3.975 Å [7] for $SrMoO_3$.

## Acknowledgments

Thanks to Tom Vogt for assistance and hospitality during the synchrotron data collection. Research carried out at Brookhaven National Laboratory in the Department of Materials and Chemical Sciences is supported by the US Department of Energy, Office of Basic Energy Sciences, Division of Materials Science, under Contract no. DE-AC02-98CH10886. The National Synchrotron Light Source is also supported by the US Department of Energy Division of Chemical Sciences.

## References


[1] J.B. Torrance, P. Lacorre, C. Asavaroengchai, R.M. Metzger, Physica C (Amsterdam) 182 (1991) 351–364.
[2] B.L. Chamberland, P.S. Danielson, J. Solid State Chem. 3 (1971) 243–247.
[3] G.H. Bouchard, M.J. Sienko, J. Michell, Inorg. Chem. 7 (1968) 441–443.
[4] K. Kamata, T. Nakamura, T. Sata, Chem. Lett. 1 (1975) 81–86.
[5] I. Nagai, N. Shirakawa, S. Ikeda, R. Iwasaki, H. Nishimura, M. Kosaka, Appl. Phys. Lett. 87 (2005) 024105/1–024105/3.
[6] J.J. Sprague, H.L. Tuller, J. Eur. Ceram. Soc. 19 (1999) 803–806.
[7] V.A. Fotiev, G.V. Bazuev, V.G. Zubkov, Izv. Akad. Nauk SSSR, Neorg. Mater. 23 (1987) 1005–1008.
[8] A.C. Larson, R.B. Von Dreele, Los Alamos National Laboratory Report LAUR, 1994.
[9] A.M. Glazer, Acta Crystallogr. Ser. B 28 (1972) 3384–3392.
[10] M.W. Lufaso, P.M. Woodward, Acta Crystallogr. Ser. B 57 (2001) 725–738.
[11] P.W. Selwood, Magnetochemistry, Interscience Publishers, New York, 1956, p. 78.
[12] H. Falcón, J.A. Alonso, M.T. Casais, M.J. Martínez-Lope, J. Sánchez-Benítez, J. Solid State Chem. 177 (2004) 3099–3104.
[13] I.H. Inoue, N. Shirakawa, I. Hase, O. Goto, H. Makinol, M. Ishikawa, J. Phys.: Condens. Matter 10 (1998) 11541–11545.
[14] S.I. Ikeda, N. Shirakawa, Physica C (Amsterdam) 341–348 (Pt. 2) (2000) 785–786.
[15] Y.C. Lan, X.L. Chen, M. He, J. Alloys Compd. 354 (2003) 95–98.
[16] H.W. Eng, P.W. Barnes, B.M. Auer, P.M. Woodward, J. Solid State Chem. 96 (2003) 535–546.
[17] S. Hayashi, R. Aoki, T. Nakamura, Mater. Res. Bull. 14 (1979) 409–413.
[18] V. Giannakopoulou, P. Odier, J.M. Bassat, J.P. Loup, Solid State Commun. 93 (1995) 579–583.
[19] L.H. Brixner, J. Inorg. Nucl. Chem. 14 (1960) 225–230.
[20] R.D. Shannon, Acta Crystallogr. Ser. A 32 (1976) 751–767.
[21] J. Garcia-Jaca, J.L. Mesa, M. Insausti, J.I.R. Larramendi, M.I. Arriortua, T. Rojo, Mater. Res. Bull. 34 (1999) 289–301.